Glacial activity and paleoclimatic evolution records in the Cosmonaut Sea since the last glacial maximum

Dong Chen[1,2], Qian Ge[1,2]*, Ziyan Lei[3], Bingfu Zhou[1,2] and Xibin Han[1,2]

[1]Key Laboratory of Submarine Geosciences, Ministry of Natural Resources, Hangzhou, China, [2]Second Institute of Oceanography, Ministry of Natural Resources, Hangzhou, China, [3]Department of Oceanography and Coastal Science, Louisiana State University, Baton Rouge, LA, United States

This research explored the origin and paleoenvironmental significance of sediments from the Cosmonaut Sea, Antarctica, focusing on the period since the Last Glacial Maximum (LGM, 26,000 cal a BP). Sediment samples from core ANT37-C5/6-07 were subjected to AMS[14]C dating, clay-mineral assemblage analysis, grain size evaluation, and geochemical testing. Results indicated illite as the dominant clay mineral (average 46%), followed by kaolinite (22%) and smectite (21%), with chlorite (11%) being the least abundant. Comparison with previous studies suggested that these sediments are largely derived from weathered material from Prydz Bay and Enderby Land coastal regions. The study of mineral ratios, geochemical elements, and sediment grain size, alongside $\delta^{18}O$ values from the East Antarctica EDML ice core, revealed that the ice sheet in the study area retreated around 18600 cal a BP, melted more markedly during 16800-15000 cal a BP, tended to expand during 14800-13500 cal a BP, and then the ice sheet remained in a state of retreat until it expanded again around 5000 cal a BP. It is largely synchronous with the phased changes in the Antarctic climate since the LGM (26ka) of the Cosmonaut Sea. Notably, the sediment record aligns with major paleoclimatic events, including Heinrich Stadial 1 and the Younger Dryas in the northern hemisphere and the Antarctic cold reversal, reflecting a climatic 'seesaw' effect. These findings suggest that the sedimentary record in the Cosmonaut Sea is a sensitive indicator of climatic conditions, highlighting a history of glacial movements and revealing East Antarctica's climatic fluctuations. Additionally, the research indicates that the regional ice sheet is more sensitive to climatic changes than previously believed, underscoring its instability.

KEYWORDS

Cosmonaut Sea, clay minerals, last glacial maximum, paleoclimate, sediment sources

Highlights

- Sources of sediment from core ANT37-C5/6-07 were analyzed;
- The warm and cold variations in the study area were reconstructed;
- Clay minerals and geochemical elements in the Antarctic sediments are good indicators of provenance and paleoclimate.

1 Introduction

Climate change on Earth has been significant in the last century, mainly characterized by global warming, which has led to the retreat of glaciers, the rise of the snow line, and the rise of the sea level at high latitudes. Being one of the most responsive areas to global climate change and a vital region for the global exchange of CO_2 between sea and air, the Southern Ocean is influential in that alterations in its climate and environment directly influence the thickness of the ice sheet and the extent of sea-ice coverage. These changes, in turn, affect ocean circulation and sea-level height, and they play a significant role in the global carbon cycle (Legendre, 1998; Collier et al., 2000; Leonardo et al., 2000). Therefore, historical changes in the Antarctic paleo-ice sheet provide insights into past climatic variations and sea-level fluctuations. Being the largest solid water reservoir on Earth, the Antarctic ice sheet constitutes approximately 90% of the world's land ice and 80% of the world's total freshwater (Ju, 2019). Satellite observations indicate melting of the Antarctic ice sheet in recent decades has contributed to a global sea-level rise of 7.6 ± 3.9 mm. The pace of sea-ice loss is progressively accelerating, and climate models predict a reduction in the sea-ice extent by approximately one-third by the end of this century (Turner et al., 2017; Rignot et al., 2019). The melting of the Antarctic ice sheet has affected the distribution of sea ice in the Southern Ocean, which, in turn, has affected ocean-air exchange, the global heat balance, and ocean circulation. Therefore, comprehending the mechanisms of interaction between the climate and glaciers in the Southern Ocean is crucial for obtaining insights into the future of the Antarctic and global climate.

Environmental changes in East and West Antarctica are showing distinct trends. Recent satellite observations indicate rising temperatures and melting sea ice in the West Antarctica, while sea ice in the East Antarctica remains relatively stable. Many scholars have conducted extensive research on the Antarctic climate, sea ice, and productivity (Bonn et al., 1998; Shepherd et al., 2004; Ducklowa et al., 2008). However, studies based on satellite observations typically only capture short-term changes in sea ice. Research on longer timescales often involves reconstructing paleo-topographic features or using proxies from marine sediments. For example, Kim et al. (2021) examined the effect of El Niño-Southern Oscillation and Circumpolar Deep Water on ice-shelf melting in the Amundsen Sea. They conducted their analysis by examining total organic carbon, total sulfur, and biogenic silicon in sediments from the Amundsen Sea. Pedro et al. (2011) explored the coupling of millennial-scale climate changes in the Antarctica and Greenland using five high-resolution Antarctic ice-core records and examining changes in global methane concentrations. Crosta et al. (2008) reconstructed climate change in the East Antarctica since the Holocene by analyzing the response of diatom species in the East Antarctic cores to seasonal climate changes.

Clay minerals in Antarctic sediments have been the focus of extensive research by scholars as a valuable tool for reconstructing paleoclimatology and interpreting sedimentary sources and processes (e.g. Biscaye, 1965; Chamley, 1997). For instance, Ehrmann et al. (1992) synthesized findings from various scholars on Antarctic clay minerals, revealing distinct clay-mineral assemblages in sediments from different seas. Understanding the variations in these assemblages and their influencing factors is essential for deciphering Antarctic paleoclimatology and changes in ice sheets.

The Cosmonaut Sea is situated in the northwestern part of the East Antarctic Enderby Land, spanning from 30°E to 60°E. It is bordered by the Reeser-Larsen Sea to the west and the Cooperative Sea to the east. Three bays, namely Lützow-Holm Bay, Casey Bay, and Amundsen Bay, are arranged from west to east. This region serves as a crucial junction for polar circulation, where dynamic physical processes like current flows and the formation and dissolution of polynyas occur. Here, the interplay between sea ice and the ocean is a dominant force in shaping the Antarctic ecosystem. The currents, sea ice and surface productivity in this area have also been analysed and studied by previous authors. Williams et al. (2010) conducted an analysis based on the BROKE-WEST survey, examining the large-scale circulation, water masses, and fronts on the inner shelf slope and the surface of upwelling areas in the Cosmonaut Sea. They observed that the sea ice in the region is complex and highly variable, characterized by multiple polynyas. Additionally, the study found that the region's dynamics are influenced by several currents: the eastward-flowing Antarctic Circumpolar Current (ACC) to the north and the westward-flowing Coastal Current and Antarctic Slope Current (ASC) to the south (see Figure 1). Additionally, the seasonal flow of Antarctic Bottom Water exists at the base of the region, and two large-scale circulations, the Prydz Bay circulation in the east and the East Weddell circulation in the west (Bibik et al., 1988), contribute to the dynamic oceanic system. And the Cosmonaut Sea is very active in physical processes, with large-scale latitudinal and meridional ocean circulation patterns, annual formation and disappearance of sea ice, and pronounced seasonal surface water mass transitions (Gloersen et al., 1993; Bindoff et al., 2000; Williams et al., 2008). Li et al. (2021) reveal the climatic response of the ice-proximal environment to the melting of the ice sheet from the Last Glacial Maximum (LGM) to Holocene based on diatom data from sediments. The knowledge of the Cosmonaut Sea in the East Antarctica is limited by previous studies, in particular, studies of the Astronaut Sea have focused on hydrology and biology, and the sedimentary record of the Cosmonaut Sea through inorganic geochemistry is relatively scarce. This research gap emphasizes the necessity of gaining a deeper understanding of the importance of the Southern Ocean
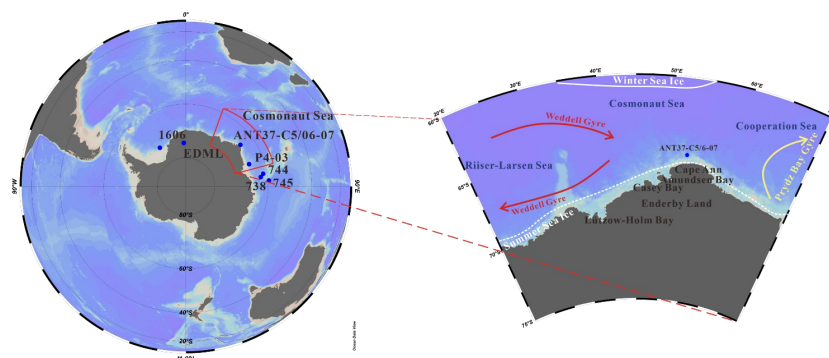
FIGURE 1
Map of the currents and core locations. The map on the left side is an overall view of the Antarctica. The map on the right side is a detailed one of the study area. The arrows represent the currents. The yellow arrow represents the Prydz Bay Gyre, the red arrows represent the Weddell Sea Gyre, the blue arrow represents ASC, the purple arrow represents ACC, the white dashed line is the summer sea-ice line, and the white solid line is the winter sea-ice line.

mineral assemblages in Antarctic paleoclimatology and glacial reconstruction, and investigating climate and sea-ice changes in the Cosmonaut Sea can significantly contribute to comprehending environmental changes in the broader Antarctica. Hence, this study focused on marine sediments from core ANT37-C5/6-07 in the Cosmonaut Sea (Figure 1) to reconstruct the paleoclimatic evolutionary history since the Last Glacial Maximum (LGM) in the East Antarctica through the analysis of clay-mineral assemblages and their integration with variations in grain size and geochemical elements.

2 Materials and methods

The samples were collected from core ANT37-C5/6-07 (52° 35.69'E, 65°21.27'S; Figure 1; recovery length: 378 cm), which was obtained during the 37th Chinese Antarctic Expedition in 2021. This station is situated in the Cosmonaut Sea at a water depth of 2825 m. For this study, a 91-cm-long sample at the top was chosen from the initial section. The sediments in this core exhibit an olive-green color and consist of silty mud that is weakly cohesive. Owing to the lack of calcareous fossils in the sediments, sediments from the Antarctic marginal sea are usually dated using the AMS[14]C method, which uses the acid-insoluble organic fraction from the sediments (Licht and Andrews, 2002; Hillenbrand et al., 2010; Hu et al., 2022),

and ages determined by this method are usually considered reliable (Licht and Andrews, 2002). Therefore, we selected samples from five layers (Table 1) for AMS[14]C dating at the Beta Analytic Inc, USA.

The pretreatment, separation, preparation, and X-ray diffraction (XRD) analysis of clay mineral samples were conducted at the Key Laboratory of Submarine Geosciences, Ministry of Natural Resources in Hangzhou, Zhejiang Province. The remaining samples, extracted from grain-size fractions smaller than 2 μm using Stokes low of sedimentation, were then transformed into oriented slices for XRD analyses. The clay-mineral profiles were analyzed and calculated using Jade 6.0. Qualitative analysis was conducted through a comprehensive comparison of the characteristics of the three oriented-sheet diffraction peaks. Semi-quantitative analysis was performed using the weighting coefficients determined by Biscaye (1965). The result for illite crystallinity was determined by averaging four calculations for each sample, with error control maintained within 3%. Ninety-one samples were analyzed with a sampling interval of 1 cm.

Grain size analysis was conducted using a laser-particle-size analyzer. The laser grain size analysis was performed using a Malvern 2000 particle-size analyzer at the Key Laboratory of Submarine Geosciences, Ministry of Natural Resources in Hangzhou, Zhejiang Province. Ninety-one samples were analyzed with a sampling interval of 1 cm.

TABLE 1 Ages of the sediments from core ANT37-C5/6-07.

Station	Sample layer (cm)	Age of AMS[14]C/a	Calibrated age/cal BP	Age of old carbon/a	Calendar ages /cal BP
ANT37-C5/6-07	0–1	5300 ± 30	2118	2118	0
ANT37-C5/6-07	11–12	13,230 ± 30	11,486	2118	9368
ANT37-C5/6-07	44–45	18,210 ± 80	17,774	2118	15,656
ANT37-C5/6-07	67–68	19,810 ± 60	19,280	2118	17,162
ANT37-C5/6-07	90–91	27,830 ± 120	28,116	2118	25,998

Geochemical elements analysis was also conducted at the Key Laboratory of Submarine Geosciences, Ministry of Natural Resources in Hangzhou, Zhejiang Province. We weighed 40 mg of whole rock powder in a polytetrafluoroethylene sample cartridge. We added 0.5 ml of HNO_3 and 1.0 ml of HF. Then, we sealed the cartridge with a steel sleeve and placed it in an oven at 195°C for 3 d. We steamed the sample bomb containing the digestion solution on a hot plate until the salt was wet. Next, we added 1 ml of HNO_3 and 4 ml of 18.2 MΩ pure water to the bomb. We resealed the bomb and placed it in a 190° C oven for 12 h of closed digestion. We removed the inner liner after cooling. Thermo Fisher's ICAP-RQ ICP-MS instrument was used to analyze the samples. The samples were collected at a 1-cm interval, and a total of 91 samples underwent testing and analysis.

3 Results

3.1 Chronology

Table 1 presents the results of AMS ^{14}C dating for the five layers. Results from acid-insoluble organic matter dating in sediments using the AMS[14]C method are usually affected by old carbon and therefore need to be calibrated. After calibration with the Calib 8.2.0 program (Stiver and Reimer, 1993) using the Marine20 dataset (Heaton et al., 2020) and adopting an ΔR value of 1120 for carbon-reservoir correction, the top age of the core was determined to be 2118 cal a BP, and the bottom age as 28,116 cal a BP (Yoshida and Moriwaki, 1979; Takano et al., 2012). In line with previous studies (Pudsey et al., 2006; Andrews et al., 2017; Hu et al., 2022), we generally performed age correction by subtracting the age at the top of the core. Owing to the proximity of the core ANT37-C5/6-07 sediments to the study location of Hu et al. (2022), we also treated the surface deposits as modern, resulting in an age of 0 cal a BP at the core's top and an old carbon age of 2118 a. Corrections involved subtracting the old carbon age and making appropriate adjustments to derive the final calendar age. The sediment-age framework for core ANT37-C5/6-07 referenced the work of Hu et al. (2023) (Figure 2).

3.2 Clay minerals

Figure 3 illustrates the contents and variations of clay minerals from core ANT37-C5/6-07. Among the clay minerals, illite exhibits the highest content, ranging from 29% to 61%, with an average of 45.98%. Illite content exhibits significant fluctuations between 40 and 60 cm, with minor changes from 0 to 40 cm. The overall variation in smectite content is relatively insignificant, ranging from 12% to 35%, averaging at 21%. Observable peaks and valleys are present in the curves to depict its content change, predominantly occurring at depths between 40 and 60 cm. Kaolinite content ranges from 15% to 30%, averaging at 22%. Below 60 cm, its content is relatively lower; however, above 60 cm, it increases and exhibits fluctuations. Chlorite content ranges from 7% to 16%, averaging at 11%. It is lower and more stable compared with the others. Overall, the fluctuation is minimal below 60 cm, with slight fluctuations observed above 60 cm. The highest content is situated at approximately 40 cm. Illite crystallinity varies from 0.31°Δ2θ to 0.53°Δ2θ. Small variations are observed below 60 cm and above 40 cm, all below 0.4°Δ2θ, indicating better crystallization. Larger variations are noted from 40 to 60 cm, exceeding 0.4°Δ2θ and indicating worse overall crystallization. The chemical index of illite ranges from 0.02 to 0.21, with a mean value of 0.06. Overall, all values are less than 0.1, with a peak around 45 cm, indicating enhanced chemical weathering. However, the overall trend suggests weathering predominantly dominated by physical weathering and controlled by cold and dry climatic conditions in the Antarctica.

3.3 Grain size

Figure 4 illustrates the vertical variation of grain size characteristic parameters in core ANT37-C5/6-07. By using the Udden-Wentworth grain-size classification method (Gladstone et al., 2001), we selected three grain-size parameters: the percentage content of grain-size fractions less than 4 μm, 4–63 μm, and greater than 63 μm. These parameters represent the percentage content of the clay, silt, and sand fractions in the samples. Silt dominated the sediments in this core,
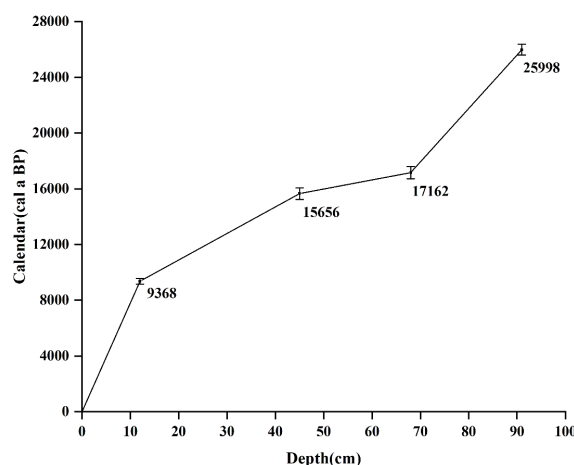

FIGURE 2
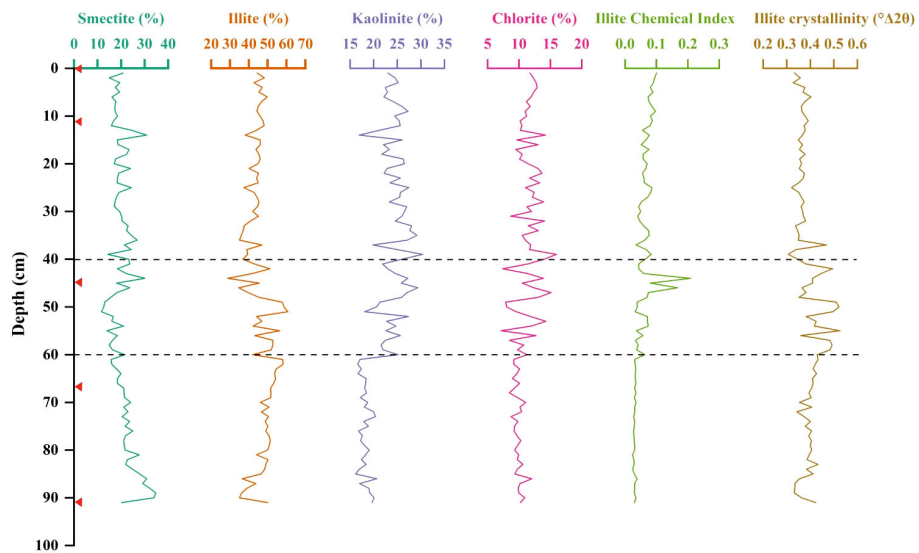Calibrated calendar ages for the top 91 cm of core ANT37-C5/6-07.

FIGURE 3
Characteristics of clay-mineral assemblages and their vertical variations in core ANT37-C5/6-07. The red triangles are age marker points.

with the average percentage of clay-component contents at 21.0% (7.1–32.2%), the average percentage of silt component contents at 58.0% (34.3–67.2%), and the average percentage of sand-component contents at 21.0% (2.4–51.9%). The variations in silt- and clay-component contents were similar but were opposite to those of sand-component contents. The mean grain size (Mz) ranged from 7.2 μm to 90.5 μm, experiencing more frequent fluctuations between 45 cm and 91 cm and then stabilizing and increasing above 45 cm. In addition, the grain size characteristics of sediments can reflect

hydrodynamic conditions and ice-rafted debris content variations (Bischof et al., 1996; Chen et al., 2014). However, using grain size data to infer depositional environments introduces some uncertainty. To mitigate this, a statistical approach—grain size-standard deviation —is often applied to enhance the interpretation of grain size data (Chen et al., 2013). This method's analysis (Figure 5) reveals three significant deviation peaks at 14.6 μm, 58.3 μm, and 1230 μm, along with three minor peaks at 0.22 μm, 25.4 μm, and 406.1 μm in the sediment of core ANT37-C5/6-07. Thus, the sediment can be
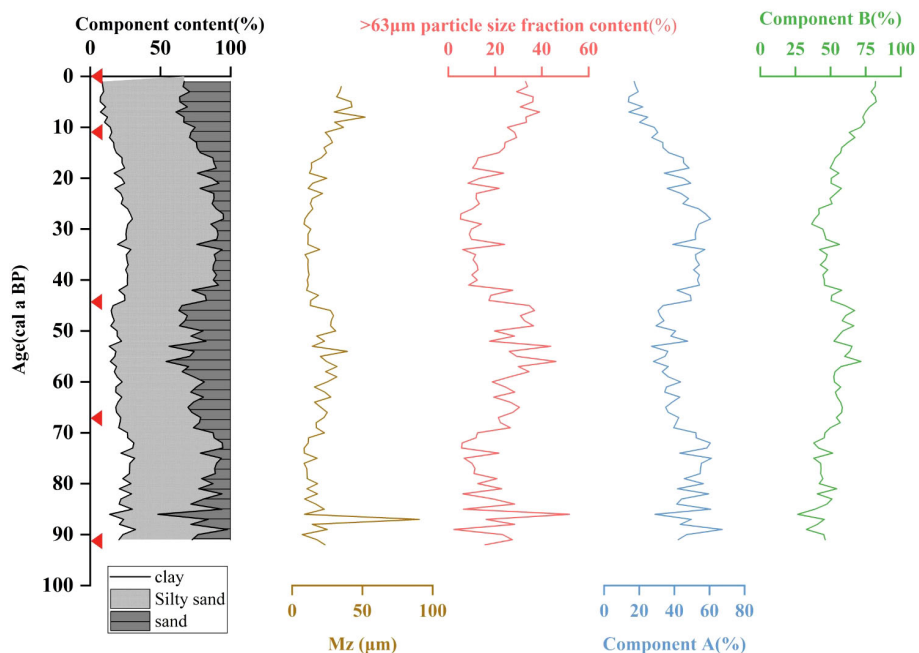

FIGURE 4
Vertical variations in the characterization of grain size in core ANT37-C5/6-07. The red triangles are age marker points.
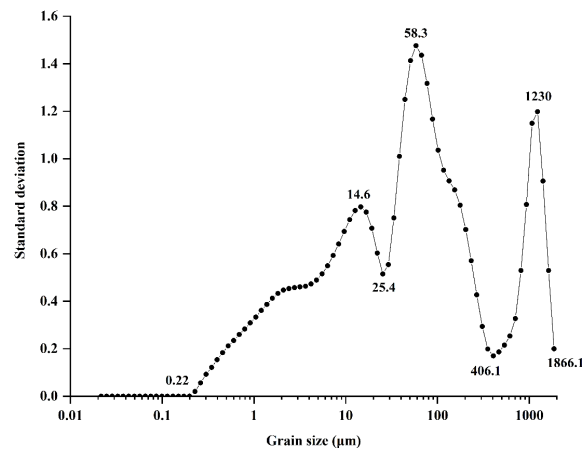
Grain size standard deviation diagram of the sediments in core ANT37-C5/6-07.

classified into three environmentally sensitive grain size groups: 0.22–25.4 µm (component A), 25.4–406.1 µm (component B), and 406.1–1866.1 µm (component C). Among these, component C is minor and exhibits a standard deviation near zero, rendering its discussion irrelevant.

3.4 Geochemical elements

Table 2 presents the results of elemental analyses for the sediments in core ANT37-C5/6-07. The contents of Al_2O_3 and Fe_2O_3 are the highest. Aluminum is commonly considered an element enriched by terrestrial-source debris. Its coefficient of variation is very small (0.06), making it suitable as a standardized element to mitigate the influence of terrestrial-source debris on elemental content. The results reveal a high coefficient of variation for the redox-sensitive element Mo and an elevated content of Ba among the trace elements in core ANT37-C5/6-07. The average concentrations are 231.73 ppm for total rare-earth elements (REE), 213.09 ppm for light rare-earth elements (LREE), and 18.64 ppm for heavy rare-earth elements (HREE). The trends reflect a

remarkable accumulation of LREE. The alterations in the characteristics of certain elements in the sediment samples from core ANT37-C5/6-07 are illustrated in Figure 6. The variations in the characteristics of elements in the sediments manifested in two distinct phases: the last glacial period and the Holocene, exhibiting significant cyclic fluctuations. Notably, except for the elements Ba and Mn, a sudden change occurred in the other elements at around 46 cm. The characteristics of terrestrial enrichment elements depicted in Figure 6, including Ti, Al, Fe, K, P, and Mg, exhibit a similarity to the trend of changes in other elemental characteristics and show a positive correlation. Conversely, Si and Ba display a negative correlation.
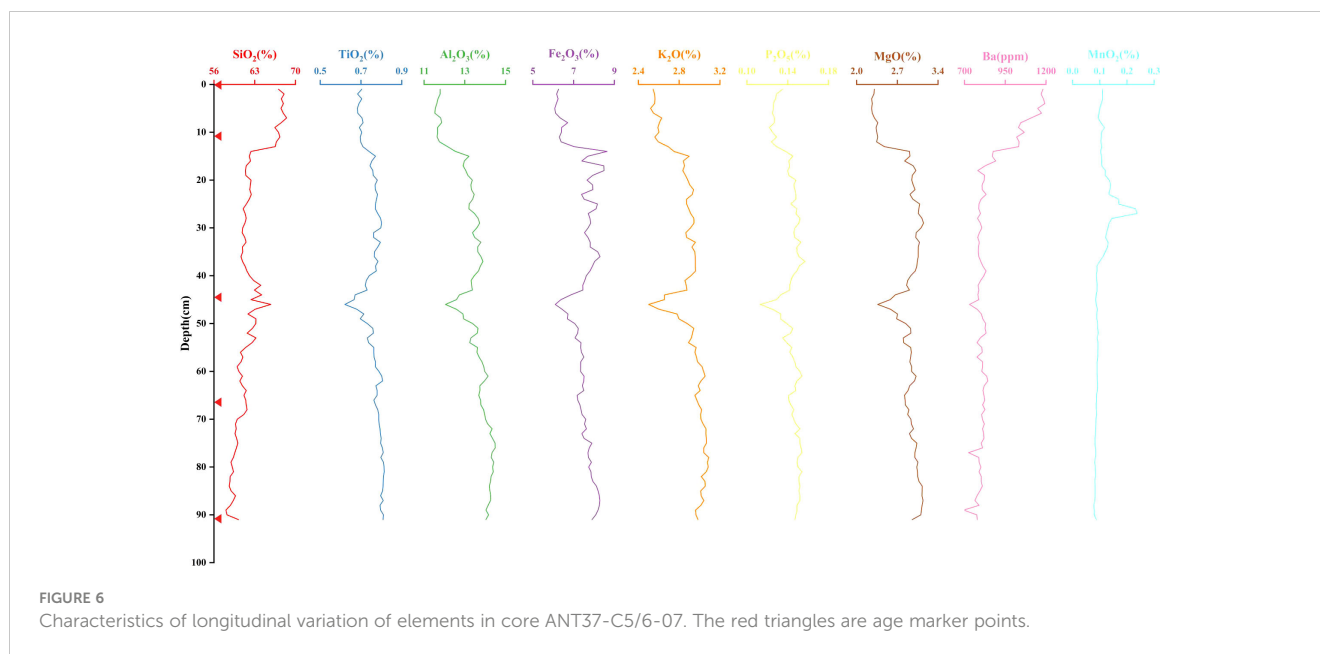
4 Discussion

4.1 Origin of sediments

Sediments in high-latitude marine environments are frequently transported by glaciers and ocean currents, encapsulating valuable insights into alterations in source areas and depositional processes. As

TABLE 2 Statistical characterization of the main and trace elements contents of the sediments from core ANT37-C5/6-07.

Elements	Mean value	Standard deviation	Variation coefficient	Elements	Mean value	Standard deviation	Variation coefficient
Al_2O_3 (%)	13.40	0.83	0.06	Mo (ppm)	0.59	0.38	0.64
TFe_2O_3 (%)	7.45	0.63	0.08	Ni (ppm)	52.73	8.34	0.16
K_2O (%)	2.89	0.16	0.06	Ba (ppm)	845.25	112.12	0.13
MgO (%)	2.87	0.26	0.09	U (ppm)	1.88	0.62	0.33
TiO_2 (%)	0.76	0.04	0.05	Th (ppm)	19.63	1.56	0.08
CaO (%)	2.58	0.27	0.10	ΣREE (ppm)	231.73	14.97	0.06
P_2O_5 (%)	0.14	0.01	0.06	ΣLREE (ppm)	213.09	14.61	0.07
MnO (%)	0.10	0.03	0.27	ΣHREE (ppm)	18.64	0.93	0.05
Co (ppm)	19.36	1.91	0.10				

FIGURE 6
Characteristics of longitudinal variation of elements in core ANT37-C5/6-07. The red triangles are age marker points.
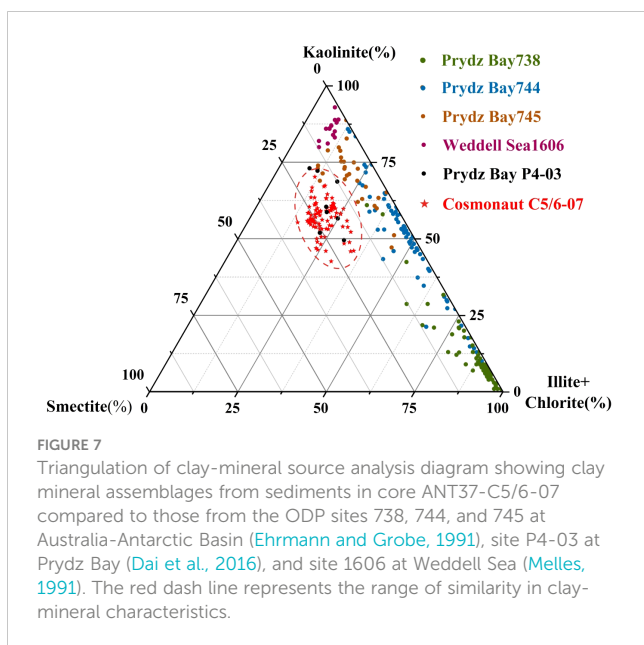
highlighted earlier, the clay-mineral composition and characteristics of impeccably preserved sediments bear information regarding depositional sources and climatic changes. However, discussions regarding the sediment source based solely on clay-mineral characteristics may be prone to bias owing to the influence of multiple mechanisms (Singer, 1984; Yemane et al., 1996). And REEs have been widely used as useful and reliable provenance proxy for terrigenous sediments from different regions (Taylor and McLennan, 1985; Xu et al., 2021). Therefore, based on the analysis of the characteristics of the clay-mineral assemblage, combined with the REE characteristics of the sediments, and compared with the characteristics in the sediments of the neighboring seas, we could identify the origin of sediments in core ANT37-C5/6-07.

The analysis of previous experimental results (Figure 3) showed that illite dominated as the clay mineral in core ANT37-C5/6-07. This dominance can be attributed to the terrestrial physical weathering and glacial abrasion processes characteristic of high-latitude regions. Illite primarily originates from the physical weathering of metamorphic and sedimentary rocks in the surrounding land. Experimental results show that the average illite crystallinity is less than 0.4°Δ2θ, indicating superior crystallization. Additionally, the illite chemical-weathering index (<0.2) suggests that the illite is mainly from physical weathering. Notably, Trail and McLeod (1969) observed that the region is predominantly composed of migmatite and gneiss. They further noted that substantial quantities of readily weatherable hydrocarbon source rocks can contribute to the presence of illite and chlorite. Smectite is typically considered a product of seafloor weathering of volcanic material, as observed in sediments from the Ross Sea. This volcanic material originates from the nearby McMurdo volcano (Jung et al., 2021). Smectite has also been identified in some Antarctic soils (Claridge, 1965), suggesting its potential presence in sediments due to the transport of ancient, loosely weathered products and soils into the ocean by glaciers or turbidity currents. Kaolinite typically forms through the chemical weathering of rocks in warm, humid temperate-to-tropical climates. However, in the cold, arid

climate of the Antarctic continent, characterized by weak chemical weathering, glaciers likely transported kaolinite from the soils and loose sediments of coastal plains from the Mesozoic to the Tertiary (Hambrey et al., 1991). Ehrmann et al. (1992) identified the presence of high levels of kaolinite in sediments from the Oligocene period, coinciding with the formation of ice sheets in the East Antarctica. After the ice sheet formed, unconsolidated debris was transported away from the continents, leaving glaciers to primarily erode unweathered rock, which resulted in only a small quantity of kaolinite being produced. Additional kaolinite likely resulted from the weathering of preexisting kaolinite-bearing sediments and the erosion of ancient soils (Trail and McLeod, 1969). Moreover, the Lambert Glacier and Emery Ice Shelf in the Prydz Bay were found to be filled with older kaolinite. When the glacier melted, the older kaolinite beneath was exposed, and subsequent weathering and erosion contributed to the kaolinite content.

Sediment provenance is further examined by considering the potential source areas of the four clay minerals and analyzing the clay-mineral assemblages. Given that both illite and chlorite result from physical weathering (Ehrmann et al., 1992), we combined their contents as a composite end member to explore their potential source regions. This analysis involved comparing them with clay mineral characteristics of other marine sediments that may share the same sediment source station (Ehrmann, 1991; Melles, 1991; Dai et al., 2016) and integrating this information with the current characteristics of the study area. The source analysis triangulation for clay minerals is shown in Figure 7. The comparison of results reveals that the clay mineral assemblages in core ANT37-C5/6-07 exhibit a distinct signature, which only partially matches that of the clay mineral assemblages from core P4-03 in Prydz Bay. This suggests that the primary source of clay minerals in core ANT37-C5/6-07 is likely nearby Enderby Land, with a portion also possibly originating from the coastal land along Prydz Bay. Referring to the core locations and current characteristics illustrated in Figure 1, both cores fell within the influence of the eastward ASC. The ASC, driven by the horizontal gradient pressure of the Antarctic Slope

FIGURE 7
Triangulation of clay-mineral source analysis diagram showing clay mineral assemblages from sediments in core ANT37-C5/6-07 compared to those from the ODP sites 738, 744, and 745 at Australia-Antarctic Basin (Ehrmann and Grobe, 1991), site P4-03 at Prydz Bay (Dai et al., 2016), and site 1606 at Weddell Sea (Melles, 1991). The red dash line represents the range of similarity in clay-mineral characteristics.
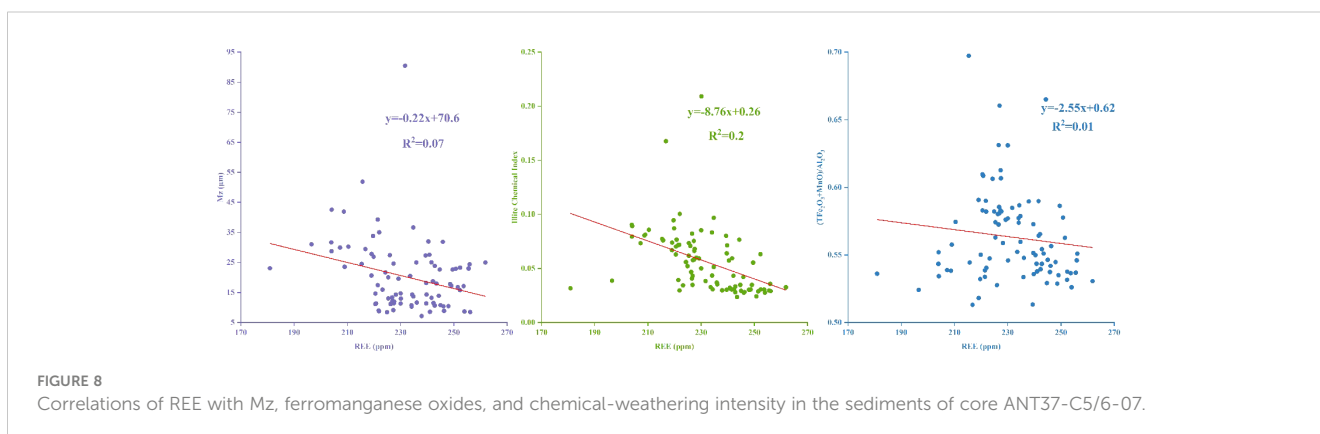
Peak, exhibits a high flow velocity, reaching a maximum of 25 cm/s and being particularly active at a water depth of 750–1250 m. Below this depth, the flow velocity gradually decreases, facilitating the deposition of detrital material (Hunt et al., 2007; Williams et al., 2010). As both cores are situated at water depths below 2500 m, their clay-mineral assemblages are significantly influenced by the ASC. Consequently, we propose that the sediments in core ANT37-C5/6-07 are partly derived from rocks weathered on the continental shelf of Prydz Bay, transported by the ASC. Additionally, some sediments are believed to originate from coastal Enderby Land. To elucidate the sediment origin further, we selected REE as proxy indicators for compositional analysis. REE is typically associated with source rocks owing to their low reactivity. However, the fractionation of REE during deposition is influenced by multiple factors. Notably, a grain size effect has been observed in REE, often leading to enrichment in fine-grained material (Cullers et al., 1987). Additionally, study results confirm the reactivity of REE during chemical weathering, where the intensity of chemical weathering can affect their composition. Moreover, REE is influenced by mineral adsorption, and research has indicated that the

composition of REE is also affected by ferromanganese oxides. Correlation analysis of the REE content of the sediments with Mz, the illite chemical index indicating chemical weathering intensity, and the $(Fe_2O_3+MnO)/Al_2O_3$ value representing ferromanganese oxide content (Dou et al., 2012) reveals that the REE content in core ANT37-C5/6-07 exhibits a weak correlation with these three factors (Figure 8). This suggests that the variation in REE features is primarily influenced by the source. Therefore, the sediment source can be inferred based on the and considering light and heavy rare-earth fractionation features, such as $(La/Sm)_N$ and $(Gd/Yb)_N$.

REE compositions in chondrite meteorites are believed to be undifferentiated. Analyzing the chondrite-normalized REE partitioning patterns can thus provide a clearer understanding of the differentiation characteristics of the sample's REE (Boynton, 1984). We compared the REE compositions in the core ANT37-C5/6-07 sediments with those in the potential source area to try to analyze the source of the sediments (Shi et al., 1998; Chen et al., 2015; Li et al., 2017; Xiu et al., 2017). The REE compositions in the core ANT37-C5/6-07 sediments, as shown in the chondrite-normalized partitioning patterns (Figure 9), display a marked enrichment in Light REE (LREE) and a depletion in Heavy REE (HREE). This pattern aligns with terrestrial source characteristics, suggesting a significant terrestrial influence, particularly from nearby Enderby Land. In contrast, the REE abundance in the sediments from the Antarctic Peninsula and Ross Island differs markedly, indicating a distinct geological origin (Shi et al., 1997; Chen et al., 2015). Moreover, the sediments in core ANT37-C5/6-07 show a higher REE content compared to those from the Ross Sea (Xiu et al., 2017). The similarity in LREE levels and the deficit in ΣHREE compared to the Enderby Land metamorphic rocks, along with distinct positive Ce anomalies and negative Eu anomalies, reflect the underlying bedrock composition, primarily ancient metamorphic rocks such as gneisses and mafic rocks (Sheraton et al., 1984; Tingey, 1991; Stagg et al., 2004). These features, supported by the bedrock characteristics in Prydz Bay and Enderby Land, suggest a mixed sediment source for core ANT37-C5/6-07.

The normalized ratios $(La/Sm)_N$ and $(Gd/Yb)_N$ indicate the fractionation levels of light and heavy rare-earth elements, respectively. A higher $(La/Sm)_N$ ratio signifies greater enrichment

FIGURE 8
Correlations of REE with Mz, ferromanganese oxides, and chemical-weathering intensity in the sediments of core ANT37-C5/6-07.
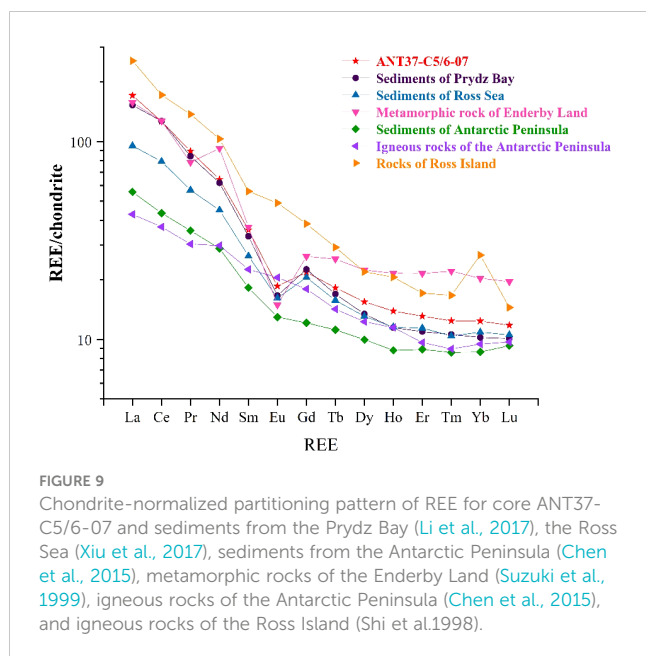
FIGURE 9
Chondrite-normalized partitioning pattern of REE for core ANT37-C5/6-07 and sediments from the Prydz Bay (Li et al., 2017), the Ross Sea (Xiu et al., 2017), sediments from the Antarctic Peninsula (Chen et al., 2015), metamorphic rocks of the Enderby Land (Suzuki et al., 1999), igneous rocks of the Antarctic Peninsula (Chen et al., 2015), and igneous rocks of the Ross Island (Shi et al.1998).

in LREEs, while a lower $(Gd/Yb)_N$ ratio points to greater HREE enrichment. By comparing the REE ratios in the sediments to those in potential source rocks, we can assess the fractionation between HREEs and LREEs. In core ANT37-C5/6-07 sediments (refer to Figure 10), the $(La/Sm)_N$ and $(Gd/Yb)_N$ ranges overlap with those from the Enderby Land Metamorphic Rocks and Prydz Bay sediments. This overlap suggests that these locations are the primary sources, as supported by the REE partitioning patterns observed.

In conclusion, the integrated analysis results of clay-mineral assemblages and REE composition strongly suggest that the
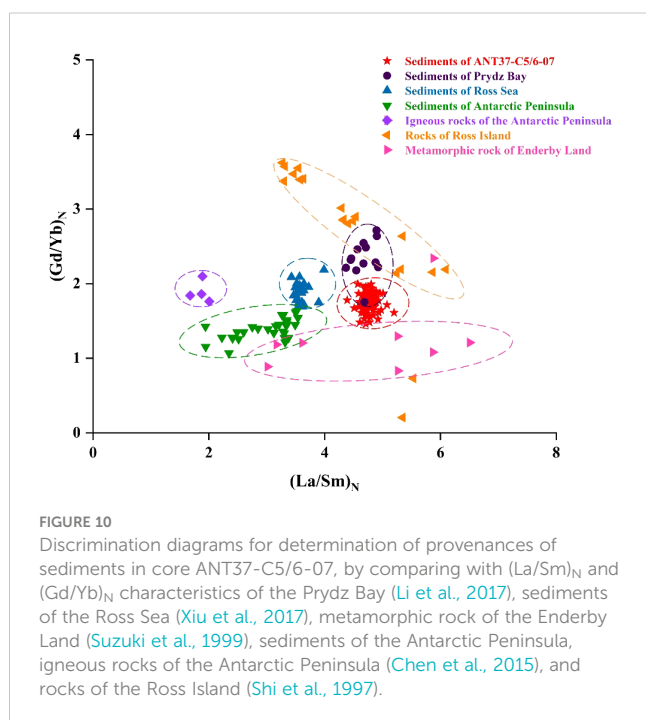

FIGURE 10
Discrimination diagrams for determination of provenances of sediments in core ANT37-C5/6-07, by comparing with $(La/Sm)_N$ and $(Gd/Yb)_N$ characteristics of the Prydz Bay (Li et al., 2017), sediments of the Ross Sea (Xiu et al., 2017), metamorphic rock of the Enderby Land (Suzuki et al., 1999), sediments of the Antarctic Peninsula, igneous rocks of the Antarctic Peninsula (Chen et al., 2015), and rocks of the Ross Island (Shi et al., 1997).

predominant source of sediments in the study area is coastal land of Prydz Bay and Enderby Land. We consider that the sediments primarily originate from coastal-land weathering, transported into the ocean through processes like glacial or turbidite deposition, and subsequently carried by the ASC before settling at this specific station.

4.2 Paleoclimatic significance since LGM

Clay-mineral assemblages in marine sediments from distinct regions convey varied climatic information. Considering the stability of ASC influencing the deposition of core ANT37-C5/6-07 (Williams et al., 2010), we propose that alterations in the clay-mineral characteristics of the sediments may indirectly indicate paleoclimatic changes. Drawing from prior studies, we propose that the smectite in the study area may have an authigenic origin, potentially affecting the accuracy of the paleoclimate information it contains (Iacoviello et al., 2010). In contrast, kaolinite originates from old kaolinite buried under glaciers or formed through chemical weathering under warm and humid climatic conditions, signifying a warm climate. Illite and chlorite result from physical weathering, typically indicating dry and cold climates. Thus, the (illite + chlorite)/kaolinite value can serve as a proxy indicator of paleoclimatology, reflecting the shift between warm and cold climates in the source area (Yang et al., 2022). Combined with other paleoclimatic proxies, we can further elucidate the reasons for the alteration of clay-mineral assemblages and changes in depositional processes to reconstruct the paleoclimatology of the source region.

The geochemical elemental characteristics of the sediments bear information about paleoenvironmental changes. The contents of various grain size fractions were analyzed through an R-type factor analysis with the sediment elements at this station (Table 3). The chosen rotation method for factor analysis was the maximum-variance rotation method, leading to the identification of two primary factors, F1 and F2. Examination of Table 3 reveals that the variance factor of F1 was larger than that of F2, signifying that F1 predominantly influenced the composition of sediment elements. The TiO_2, Al_2O_3, Fe_2O_3, MgO, K_2O, P_2O_5, and clay fractions displayed high positive loadings, denoting their typical characteristics as terrigenous inputs. The iron could be correlated with chlorite, illite, and smectite, while potassium was primarily linked to potassium feldspar and illite. The F2 factor has positive high loadings only for MnO and chalk, which may indicate that Mn is more likely to be in the silty sand grain fraction relative to the other elements (Zhang, 2011). The SiO_2 and barium constitute components of marine-derived sediments, and SiO_2 levels could be associated with diatoms. Previous research has demonstrated that climatic variations can influence the timing and extent of sea-ice coverage in the Southern Ocean, subsequently influencing the photosynthesis of surface phytoplankton (Wong et al., 1999; Ducklowa et al., 2008). Therefore, biogenic barium (Ba_{bio}) and Si/Al were chosen as paleo-productivity indicators to indirectly infer information on climate warming and cooling. The Ba_{bio} was calculated using the following formula (Bonn et al., 1998):

TABLE 3 Results of R-type factor analysis of elements and grain size fractions from core ANT37-C5/6-07.

	F1	F2	Factor	Percentage of variance	Accumulated %
SiO$_2$	-0.968	0.008	F1	62.857	62.857
TiO$_2$	0.904	0.121	F2	20.601	83.457
Al$_2$O$_3$	0.98	-0.061			
Fe$_2$O$_3$	0.846	0.261			
MnO	-0.169	0.67			
MgO	0.953	0.179			
K$_2$O	0.966	-0.04			
P$_2$O$_5$	0.861	0.221			
Ba	-0.827	-0.004			
Clay	0.759	0.527			
Silty sand	0.094	0.943			
Sand	-0.483	-0.829			

$$Ba_{bio} = Ba_{tatal} - Al_{sed} \times (Ba/Al)_{ter}$$

where $(Ba/Al)_{ter}$ represents the abundance of barium in the terrestrial crust and has a value of 0.0051 (Taylor, 1964).

Combined with the previous section, the grain size composition and characteristics of marine sediments can indirectly reflect the hydrodynamic strength at the time of deposition, currents and other changes in the depositional environment (Hall et al., 2011). Compared with component A, the content of component B is higher, and the change of the content B shows an obvious positive correlation with the average grain size change of the sediment in the core ANT37-C5/06-07, which indicates that the change of the content B influences the overall change of the grain size of the sediment, and it is more sensitive to the environmental changes. Therefore, this paper suggests that component B can be used as a proxy indicator for changes in the depositional environment, and that the grain size components A and B correspond to the environmentally sensitive clay and silt, which to some extent can be indicative of weak and strong hydrodynamic conditions.

The ebb and flow of glaciers are deeply intertwined with shifts in climate patterns. Studies, including Stammerjohn et al. (2015), have demonstrated that rising temperatures significantly influence ice melt. This melting corresponds with periods of glacial retreat, often associated with warmer climates, which in turn fosters the emergence of open oceanic environments and an increase in surface productivity. In contrast, cooler climates are marked by a reduction in this productivity due to expansive sea-ice coverage. The presence of coarser grain sizes in sediment, like those greater than 63 μm, 125 μm, and 150 μm, is frequently interpreted as an indicator of increased ice-rafted debris (Chen et al., 2006), reflecting such climatic shifts. Within the specific environmental context of the area under study, it is plausible that the kaolinite found originates from the physical weathering and erosion of ancient, glacier-buried deposits, as indicated by its concentration. Notably, this kaolinite

content aligns with the >63 μm grain size fraction, providing a sedimentary record that can be used to trace historical glacial movements.

To unravel the history of climate in Antarctica, we turned to ice cores, which are rich archives of past climatic conditions. In this study, the analysis went further, incorporating additional proxies; we delved into the intricate details of sedimentary records from core ANT37-C5/6-07. We scrutinized the variations in the composition of clay minerals, their relative proportions, the Ba$_{bio}$, the silicate-to-aluminum ratio (Si/Al), the >63 μm grain size fractions, and the component B. These sedimentary parameters were cross-referenced with the oxygen isotope data (δ^{18}O) from the EDML ice core, which was obtained near our study site (as illustrated in Figure 1; Epica Community Members, 2006). Our comprehensive approach allowed us to piece together a dynamic history of hydrodynamics, paleoproductivity, and ice cover in the region. Through this lens, we discerned four distinct periods alternating between warmer and cooler climates (labeled P1 through P4). Moreover, we pinpointed the timing of these local environmental shifts in relation to broader global climatic events, as depicted in Figure 11.

During the period from 26,000 to 18,600 cal a BP, the (illite + chlorite)/kaolinite value was relatively high, and the kaolinite content was low. These features suggest a cold climate, weak chemical weathering intensity, and the reburial of older kaolinite due to the re-formation of the ice sheet. And content of component B is consistently low, indicating a less hydrodynamic depositional environment. This may be due to the fact that the exchange between the upper and lower water column was inhibited during that period due to sea ice cover. Concurrently, reduced values of Ba$_{bio}$ and the Si/Al value point to diminished marine surface productivity, attributable to the sea ice extent. Marked variations in the >63μm grain size fraction, representing ice-rafted debris, were observed throughout this interval. Complementing these findings, the persistently low δ^{18}O values in the EDML ice core corroborate a colder climate and intensified glacial conditions. The alignment of these conditions with the Last Glacial Maximum (LGM) confirms
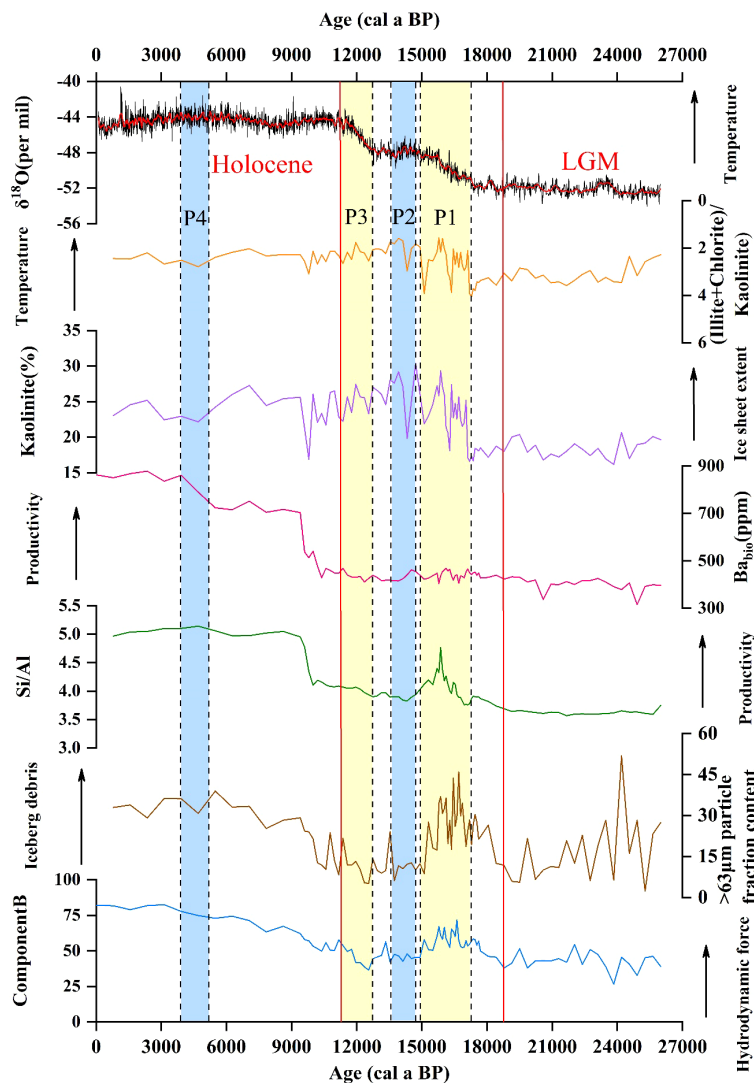
FIGURE 11
Changes in clay-mineral assemblages, Ba$_{bio}$, Si/Al, component B, content of >63-μm grain size fractions in the core ANT37-C5/6-07 sediments, and δ^{18}O of the EDML ice cores (Epica Community Members, 2006). The red line demarcates the LGM and Holocene phases, with the blue and yellow areas representing the cooler and warmer phases (P1-P4), respectively.

the chronology posited by Huybrechts (2002). Additionally, the shifts in these indicators denote that the study area commenced the Last Deglaciation around 18,600 cal a BP.

During the interval from 16,800 to 15,000 cal a BP (P1), a notable trend was observed: a decline in the (illite + chlorite)/kaolinite value to a nadir coincided with a significant rise in the δ^{18}O values of the EDML ice cores. Concurrently, the content of component B showed an upward tendency. These trends collectively suggest a warming climate. In this phase, the >63 μm grain size fraction, initially increased and then declined, mirroring the glacier retreat that first released and later reduced the transport of such debris to the study area. This glacial retreat also facilitated enhanced phytoplankton photosynthesis and wind-stressed upwelling, intensifying surface-layer productivity and hydrodynamic conditions. Additionally, weathering and erosion exposed older kaolinite previously under

the ice sheet, resulting in a significant increase in the kaolinite content. However, there was no significant change in Ba$_{bio}$, an indicator of productivity. This was attributed to a warming climate. The sudden increase in surface productivity led to the deposition of settled organic matter that consumes large amounts of oxygen, creating an anoxic environment and resulting in low levels of Ba$_{bio}$ (Hu et al., 2023).

The subsequent period between 14,800 and 13,500 cal a BP (P2) was characterized by an opposite trend: the (illite + chlorite)/kaolinite value ascended, δ^{18}O values dropped, and the >63 μm grain size fraction markedly escalated, while kaolinite content diminished. Si/Al, Ba$_{bio}$, and component B contents were comparatively low, suggesting a cooling climate, a surge in ice-rafted debris due to new ice sheet formation, and the reburial of kaolinite. And the new ice sheet resulted in restricted vertical

mixing in the water column, weaker hydrodynamics, and reduced surface productivity.

From 12,800 to 11,400 cal a BP (P3), a warming climate was once again indicated by a decrease in the (illite + chlorite)/kaolinite value, a rise in kaolinite and component B content, a decline in the >63μm fraction, and the increase in $\delta^{18}O$. Conversely, the Si/Al value and Ba_{bio} content remained relatively stable, implying lower temperatures during this warm period compared to the previous warm period. Studies by Borchers et al. (2016) in the nearby Burton Basin in East Antarctica also indicated that the ice shelf front started to retreat from the site around 12,800 cal a BP, evidencing warming during this period.

The sedimentary record in core ANT37-C5/6-07 provides a detailed account of the Antarctic climate transition from colder to warmer conditions following the Last Glacial Maximum (LGM). This transition in Antarctica was distinct from that in the Northern Hemisphere, largely because the extensive landmass of the Northern Hemisphere experienced more rapid warming during the initial phase of the last deglaciation. This led to increased ice meltwater influx into the North Pacific, causing a weakening of the Atlantic Meridional Overturning Current and consequent heat accumulation in the Southern Ocean. This heat accumulation, in turn, warmed the Antarctic climate, establishing a temperature gradient between the North and South Poles, an effect known as the Bipolar Seesaw (Broecker, 1998; Wang et al., 2015). Compared to previous studies in the East Antarctic (Borchers et al., 2016; Yang et al., 2021), the geochemical proxies in the Cosmonaut Sea, particularly the shifts in (illite + chlorite)/kaolinite values, Ba_{bio} content, Si/Al, and the content of component B in core ANT37-C5/6-07, provide a clear timeline for the Antarctic ice sheet's response to these climatic shifts. Notably, the warming in Antarctica from 16,800 cal a BP to 15,000 cal a BP (P1) occurred concurrently with the Heinrich Stadial 1 (HS1) in the Northern Hemisphere, whereas the cooler phase from 14,800 cal a BP to 13,500 cal a BP (P2) aligns with the Antarctic Cold Reversal (ACR). This latter period saw significant glacial expansion in the Ross Sea, further evidencing the frigid conditions in Antarctica (Huang et al., 2016). Following this, the period from 12,800 to 11,400 cal a BP (P3) signifies a warming phase post-ACR, which overlaps with the Younger Dryas (YD) cooling event in the Northern Hemisphere (Alley et al., 2003).

From 11,400 cal a BP to 5,000 cal a BP, the climate data from core ANT37-C5/6-07 show a phase of relative climatic stability and warming in Antarctica. The ratio of (illite + chlorite) to kaolinite was consistently low, reflecting stable conditions, while the $\delta^{18}O$ values showed minimal fluctuations, indicating steady climatic conditions. The low content of >63μm particles, representing ice-rafted debris, along with stable kaolinite content, suggests a constant source and reduced glacial activity. This period saw significant increases in Si/Al values, Ba_{bio}, and component B content, pointing to diminished sea ice, enhanced water column exchange, and heightened surface plankton photosynthesis, culminating in increased productivity. These conditions mark the gradual climatic shift into the Holocene, characterized by overall warming (Bentley et al., 2009). Post-ACR, the climate witnessed a

warming trend, with only minor fluctuations. However, between 5,000 cal a BP and 4,000 cal a BP (P4), a slight cooling is observed, as the (illite + chlorite)/kaolinite value increased, and kaolinite content decreased, which is in line with the $\delta^{18}O$ records. Despite this cooling signal, the sedimentary record from the Antarctic Peninsula by Shevenell et al. (1996) confirms a warmer paleoclimate overall for this period. Notably, Si/Al and Ba_{bio} levels remained high, indicating sustained productivity, a phenomenon attributed to the reduced influence of sea ice and increased significance of solar irradiance in the post-Holocene warm climate (Hu et al., 2023). After this colder climatic phase, the (illite + chlorite)/kaolinite value remained low and stable, while the value of Si/Al, the content of Ba_{bio} and component B were high. This indicates that the Antarctica has generally been characterized by warmer conditions and the hydrodynamic is strong, surface productivity is high in the study area, collectively, these indicators suggest the initiation of a climatically suitable period in the Antarctica.

In summary, the variations in clay mineral assemblages, grain size distributions, and elemental compositions within core ANT37-C5/6-07 from the Cosmonaut Sea have proven to be effective indicators of the historical dynamics of the ice sheet since the Last Glacial Maximum (LGM). Comparative analysis with prior studies in West Antarctica (Long et al., 2024) and East Antarctica, including future projections (Borchers et al., 2016; Yang et al., 2021), reveals that the ice sheet in our study area exhibits heightened sensitivity to climatic shifts. This sensitivity allows for more precise dating of climatic events in East Antarctica. Our findings challenge the notion of stability in the East Antarctic ice sheet as proposed by Rignot et al. (2019), suggesting that there remains a considerable risk of ice-shelf collapse under ongoing global warming.

5 Conclusions

Our comprehensive study and analysis of clay minerals, grain sizes, and elemental characteristics in the sediments from core ANT37-C5/6-07 in the Cosmonaut Sea have led to the following primary conclusions:

(1) The integration of clay mineral assemblages and REE profiles in the sediment points to a predominant influence of rock weathering from Prydz Bay and Enderby Land coastlines, indicating these areas as the main sediment sources.

(2) Based on the (illite + chlorite)/kaolinite value, content of Ba_{bio} and cpmponent B, Si/Al value, content of >63μm grain size fractions in the sediments of core ANT37-C5/6-07, and the $\delta^{18}O$ record of the EDML ice core, we found that the ice sheet in the study area retreated around 18600 cal a BP, had significant ablation during 16800-15000 cal a BP (P1) and 12800-11400 cal a BP (P3), and expanded during 14800-13500 cal a BP (P2) and 5000-4000 cal a BP (P4). It is largely

synchronous with the phases of climate changes in the Cosmonaut Sea since the LGM (26 ka). These findings align with previous Antarctic studies, offering evidence for understanding the climatic response of the Cosmonaut Sea and the East Antarctic region to global changes.

Data availability statement

The original contributions presented in the study are included in the article/supplementary material. Further inquiries can be directed to the corresponding author.

Author contributions

DC: Writing – original draft, Writing – review & editing. QG: Funding acquisition, Investigation, Project administration, Supervision, Writing – review & editing. ZL: Investigation, Supervision, Visualization, Writing – review & editing. BZ: Writing – review & editing. XH: Formal analysis, Investigation, Resources, Writing – review & editing.

Funding

Acknowledgments

Conflict of interest

The authors declare that the research was conducted in the absence of any commercial or financial relationships that could be construed as a potential conflict of interest.

Publisher's note

All claims expressed in this article are solely those of the authors and do not necessarily represent those of their affiliated organizations, or those of the publisher, the editors and the reviewers. Any product that may be evaluated in this article, or claim that may be made by its manufacturer, is not guaranteed or endorsed by the publisher.

References

Alley, R. B., Marotzke, J., Nordhaus, W. D., Overpeck, J. T., Peteet, D. M., Pielke, R. A., et al. (2003). Abrupt climate change. *Science* 299, 2005–2010. doi: 10.1126/science.1081056

Andrews, J. T., Domack, E. W., Cunningham, W. L., Leventer, A., Licht, K. J., Jull, A. J., et al. (2017). Problems and possible solutions concerning radiocarbon dating of surface marinesediments, ross sea, Antarctica. *Quater. Res.* 52, 206–216. doi: 10.1006/qres.1999.2047

Bentley, M. J., Hodgson, D. A., Smith, J. A., Cofaigh, C. Ó., Domack, E. W., Larter, R. D., et al. (2009). Mechanisms of Holocene palaeoenvironmental change in the Antarctic Peninsula region. *Holocene* 19, 51–69. doi: 10.1177/0959683608096603

Bibik, V. A., Maslennikov, V. V., Pelevin, A. S., Polonsky, V. E., and Solyankin, E. V. (1988). "The current system and the distribution of waters of different modifications in the Cosmonaut Sea," in *Interdisciplinary investigations of pelagic ecosystem in the commonwealth and cosmonaut seas* (VNIRO Publishers, Moscow), 16–43

Bindoff, N. L., Rosenberg, M. A., and Warner, M. J. (2000). On the circulation and water masses over the Antarctic continental slope and rise between 80 and 150 E. *Deep Sea Res. Part II: Topical Stud. Oceanogr.* 47, 2299–2326. doi: 10.1016/S0967-0645(00)00038-2

Biscaye, P. E. (1965). Mineralogy and sedimentation of recent deep-sea clay in the Atlantic ocean and adjacent seas and oceans. *Geol. Soc. America Bull.* 76, 803–832. doi: 10.1130/0016-7606(1965)76[803:MASORD]2.0.CO;2

Bischof, J., Clark, D. L., and Vincent, J. S. (1996). Origin of ice-rafted debris: Pleistocene paleoceanography in the western Arctic Ocean. *Paleoceanography* 11, 743–756. doi: 10.1029/96PA02557

Bonn, W. J., Gingele, F. X., Grobe, H., Mackensen, A., and Fütterer, D. K. (1998). Palaeoproductivity at the Antarctic continental margin: Opal and barium records for the last 400 ka. *Palaeogeogr. Palaeoclimatol. Palaeoecol.* 139, 195–211. doi: 10.1016/S0031-0182(97)00144-2

Borchers, A., Dietze, E., Kuhn, G., Esper, O., Voigt, I., Hartmann, K., et al. (2016). Holocene ice dynamics and bottom-water formation associated with Cape Darnley polynya activity recorded in Burton Basin, East Antarctica. *Mar. Geophys. Res.* 37, 49–70. doi: 10.1007/s11001-015-9254-z

Boynton, W. V. (1984). Cosmochemistry of the rare earth elements: meteorite studies. *Develop. Geochem.* 2, 63–114. doi: 10.1016/B978-0-444-42148-7.50008-3

Broecker, W. S. (1998). Paleocean circulation during the last deglaciation: a bipolar seesaw. *Paleoceanography* 13, 119–121. doi: 10.1029/97PA03707

Chamley, H. (1997). *Clay Mineral Sedimentation in the Ocean. In: Soils and Sediments* Vol. 623, 269-302 (Springer Berlin Heidelberg). doi: 10.1007/978-3-642-60525-3_13

Chen, Z. H., Chen, Y., Wang, R. J., Huang, Y. H., Liu, X. D., Wang, L., et al. (2014). Ice-rafted detritus events and paleoceanographic records in tne bering basin since last deglaciation. *Chin. J. Polar Res.* 26, 17. doi: 10.13679/j.jdyj.2014.1.017

Chen, Z. H., Huang, Y. H., Tang, Z., Wang, H. Z., Ge, S. L., Fang, X. S., et al. (2015). Rare earth elements in the offshore surface sediments of the northeastern Antarctic Peninsula and their implications for provenance. *Mar. Geol. Quater. Geol.* 35, 145–155. doi: 10.3724/SP.J.1140.2015.03145

Chen, Q., Liu, D. Y., Chen, Y. J., Shen, X. H., Jiang, J. J., Li, X., et al. (2013). Comparative analysis of grade-standard deviation method and factors analysis method for environmental sensitive factor analysis. *Earth Environ.* 41, 319–325. Available at: http://ir.yic.ac.cn/handle/133337/6562.

Chen, Z., Shi, X., Cai, D., Han, Y., and Yang, Z. (2006). Organic carbon and nitrogen isotopes in surface sediments from the western Arctic Ocean and their implications for sedimentary environments. *Haiyang Xuebao* 25, 16. doi: 10.3321/j.issn:0253-4193.2006.06.009

Claridge, G. G. C. (1965). The clay mineralogy and chemistry of some soils from the Ross dependency, Antarctica. *New Z. J. Geol. Geophys.* 8, 186–220. doi: 10.1080/00288306.1965.10428107

Collier, R., Dymond, J., Honjo, S., Manganini, S., Francois, R., and Dunbar, R. (2000). The vertical flux of biogenic and lithogenic material in the Ross Sea: moored sediment

trap observations 1996-1998. *Deep Sea Res. Part II: Topical Stud. Oceanogr.* 47, 3491–3520. doi: 10.1016/S0967-0645(00)00076-X

Crosta, X., Denis, D., and Ther, O. (2008). Sea ice seasonality during the Holocene, Adélie Land, East Antarctica. *Mar. Micropaleontol.* 66, 222–232. doi: 10.1016/j.marmicro.2007.10.001

Cullers, R. L., Barrett, T., Carlson, R., and Robinson, B. (1987). Rare-earth element and mineralogic changes in Holocene soil and stream sediment: a case study in the Wet Mountains, Colorado, USA. *Chem. Geol.* 63, 275–297. doi: 10.1016/0009-2541(87)90167-7

Dai, Q. Q., Wang, B. S., and Zhang, Y. P. (2016). Clay mineral composition of the Prydz Bay and its Climate implications. *Mar. Geol. Front.* 32, 6. doi: 10.16028/j.1009-2722.2016.0200

Dou, Y. G., Li, J., and Li, Y. (2012). Rare earth element compositions and provenance implication of surface sediments in the eastern Beibu Gulf. *Geochimica* 41, 147–157. doi: 10.3969/j.issn.0379-1726.2012.02.006

Ducklowa, H. W., Ericksona, M., Kellyb, J., Montes-Hugo, M., Ribic, C. A., Smith, R. C., et al. (2008). Particle export from the upper ocean over the continental shelf of the west Antarctic Peninsula: A long-term record 1992–2007. *Deep Sea Res. Part II: Topical Stud. Oceanogr.* 55, 2118–2131. doi: 10.1016/j.dsr2.2008.04.028

Ehrmann, W. U. (1991). Implications of sediment composition on the southern kerguelen plateau for paleoclimate and depositional environment. *Proc. ocean drill. Program Sci. results* 119, 185–210. doi: 10.2973/odp.proc.sr.119.121.1991

Ehrmann, W. U., and Grobe, H. (1991). Cyclic sedimentation at sites 745 and 746. *Proc. Ocean Drill. Program Sci. Results* 119, 225–237. doi: 10.2973/odp.proc.sr.119.123.1991

Ehrmann, W. U., Melles, M., Kuhn, G., and Grobe, H. (1992). Significance of clay mineral assemblages in the Antarctic Ocean. *Mar. Geol.* 107, 249–273. doi: 10.1016/0025-3227(92)90075-S

Epica Community Members (2006). One-to-one coupling of glacial climate variability in Greenland and Antarctica. *Nature* 444, 195–198. doi: 10.1038/nature05301

Gladstone, R. M., Bigg, G. R., and Nicholls, K. W. (2001). Iceberg trajectory modeling and meltwater injection in the Southern Ocean. *J. Geophys. Res. Atmosph.* 106, 19903–19915. doi: 10.1029/2000JC000347

Gloersen, P., Campbell, W. J., Cavalieri, D. J., Comiso, J. C., Parkinson, C. L., and Zwally, H. J. (1993). Satellite passive microwave observations and analysis of Arctic and Antarctic sea ice 1978–1987. *Ann. Glaciol.* 17, 149–154. doi: 10.3189/S0260305500012751

Hambrey, M. J., Ehrmann, W., and Larsen, B. (1991). Cenozoic glacial record of the Prydz Bay continental shelf, East Antarctica. *Proc. ocean drill. Program Sci. results* 119, 77–132. doi: 10.2973/odp.proc.sr.119.200.1991

Heaton, T. J., Köhler, P., Butzin, M., Bard, E., Reimer, R. W., Austin, W. E., et al. (2020). Marine20—The marine radiocarbon age calibration curve (0–55,000 cal BP). *Radiocarbon* 62, 779–820. doi: 10.1017/RDC.2020.68

Hillenbrand, C. D., Smith, J. A., Kuhn, G., Esper, O., Gersonde, R., Larter, R. D., et al. (2010). Age assignment of a diatomaceous ooze deposited in the western Amundsen Sea Embayment after the Last Glacial Maximum. *J. Quater. Sci.: Published Quater. Res. Assoc.* 25, 280–295. doi: 10.1002/jqs.1308

Hu, B. Y., Long, F. J., Han, X. B., Zhang, Y. C., Hu, L. M., Xiang, B., et al. (2022). The evolution of paleoproductivity since the Middle Holocene in the Cosmonaut Sea, Antarctic. *Earth Sci. Front.* 29, 113–122. doi: 10.13745/j.esf.sf.2022.1.12

Hu, L. M., Zhang, Y., Wang, Y. Z., Ma, P. Y., Wu, W. D., Ge, Q., et al. (2023). Paleoproductivity and deep-sea oxygenation in Cosmonaut Sea since the Last Glacial Maximum: Impact on atmospheric CO_2. *Front. Mar. Sci.* 10. doi: 10.3389/fmars.2023.1215048

Huang, M. X., Wang, R. J., Xiao, W. S., Wu, L., and Chen, Z. H. (2016). Retreat process of Ross ice shelf and Hydrodynamic changes on northwestern Ross continental shelf since the Last Glacial. *Mar. Geol. Quater. Geol.* 36, 97–108. doi: 10.16562/j.cnki.0256-1492.2016.05.010

Hunt, B. P. V., Pakhomov, E. A., and Trotsenko, B. G. (2007). The macrozooplankton of the cosmonaut sea, east Antarctica (30°E–60°E), 1987–1990. *Deep Sea Res. Part I: Oceanogr. Res. Pap.* 54, 1042–1069. doi: 10.1016/j.dsr.2007.04.002

Huybrechts, P. (2002). Sea-level changes at the lgm from ice-dynamic reconstructions of the Greenland and antarctic ice sheets during the glacial cycles. *Quater. Sci. Rev.* 21, 203–231. doi: 10.1016/S0277-3791(01)00082-8

Iacoviello, F., Giorgetti, G., Memmi, I. T., and Nieto, F. (2010). "Authigenic and detrital smectites in Cenozoic marine sediments from McMurdo continental margin (Antarctica)," in *International Polar Year - Oslo Science conference 2010*. Available at: https://www.researchgate.net/publication/294729284_Authigenic_and_detrital_smectites_in_Cenozoic_marine_sediments_from_McMurdo_continental_margin_Antarctica.

Ju, M. S. (2019). *Late Quaternary cyclic variations of ice sheet and oceanography in the Amundsen Sea sector, Antarctica* (First Institute of Oceanography, MNR)

Jung, J., Ko, Y., Lee, J., Yang, K., Park, Y. K., Kim, S., et al. (2021). Multibeam bathymetry and distribution of clay minerals on surface sediments of a small bay in Terra Nova bay, Antarctica. *Minerals* 11, 72. doi: 10.3390/min11010072

Kim, S. Y., Lim, D., Rebolledo, L., Park, T., Esper, O., Muñoz, P., et al. (2021). A 350-year multiproxy record of climate-driven environmental shifts in the Amundsen Sea

Polynya, Antarctica. *Global Planet. Change* 205, 103589. doi: 10.1016/j.gloplacha.2021.103589

Legendre, L. (1998). Flux of particulate organic material from the euphoric zone of ocean: Estimation phytoplankton biomass. *J. Geophys. Res.* 103, 2897–2903. doi: 10.1029/97JC02706

Leonardo, L., Mauro, F., Mariangela, R., and Cristina, B. (2000). Particle fluxes and biogeochemical processes in an area influenced by seasonal retreat of the ice margin (northwestern Ross Sea, Antarctic). *J. Mar. Syst.* 27, 221–234. doi: 10.1016/S0924-7963(00)00069-5

Li, G. G., Ji, Y. J., Li, Y. H., Leng, Q. N., Bu, R. Y., and Li, Y. X. (2017). Geochemical characteristics of rare earth elements in the sediments of Prydz Bay, Antarctica. *Chin. J. Polar Res.* 29, 23. doi: 10.13679/j.jdyj.2017.1.023

Li, Q. M., Xiao, W. S., Wang, R. J., and Chen, Z. H. (2021). Diatom based reconstruction of climate evolution through the Last Glacial Maximum to Holocene in the Cosmonaut Sea, East Antarctica. *Deep Sea Res. Part II: Topical Stud. Oceanogr.* 194, 104960. doi: 10.1016/j.dsr2.2021.104960

Licht, K. J., and Andrews, J. T. (2002). The ^{14}C record of late pleistocene ice advance and retreat in the central ross sea, Antarctica. *Arctic Antarctic Alpine Res.* 34, 324–333. doi: 10.1080/15230430.2002.12003501

Long, F. J., Xiang, B., Wang, Y. Z., Zhang, Y. C., Hu, L. M., Sun, X., et al. (2024). Evolution of paleoproductivity in the Antarctica Ross Sea since the Last Glacial Maximum. *Mar. Geol. Quater. Geol.* 44, 109–120. doi: 10.16562/j.cnki.0256-1492.2022111601

Melles, M. (1991). Late Quaternary paleoglaciology and paleoceanography at the continental margin of the southern Weddell Sea, Antarctica. *Polarstern Abstr.* 6, 128–129. doi: 10.2312/BzP_0081_1991

Pedro, J. B., Ommen, T. D. V., Rasmussen, S. O., Morgan, V. I., and Delmotte, M. (2011). The last deglaciation: timing the bipolar seesaw. *Climate Past* 7, 397–430. doi: 10.5194/cp-7-671-2011

Pudsey, C. J., Murray, J. W., Appleby, P., and Evans, J. (2006). Ice shelf history from petrographic and foraminiferal evidence, Northeast Antarctic Peninsula. *Quater. Sci. Rev.* 25, 2357–2379. doi: 10.1016/j.quascirev.2006.01.029

Rignot, E., Mouginot, J., Scheuchl, B., Broeke, M. V. D., and Morlighem, M. (2019). Four decades of antarctic ice sheet mass balance from 1979–2017. *Proc. Natl. Acad. Sci.* 116, 201812883. doi: 10.1073/pnas.1812883116

Shepherd, A., Wingham, D., and Rignot, E. (2004). Warm ocean is eroding west antarctic ice sheet. *Geophys. Res. Lett.* 31, 1-4. doi: 10.1029/2004GL021106

Sheraton, J. W., Black, L. P., and McCulloch, M. T. (1984). Regional geochemical and isotopic characteristics of high-grade metamorphics of the Prydz Bay area: the extent of Proterozoic reworking of Qrchaean continental crust in East Antarctica. *Precambrian Res.* 26, 169–198. doi: 10.1016/0301-9268(84)90043-3

Shevenell, A. E., Domack, E. W., and Kernan, G. M. (1996). Record of Holocene palaeoclimate change along the Antarctic Peninsula: evidence from glacial marine sediments, Lallemand Fjord. *Pap. Proc. R. Soc. Tasmania* 130, 55–64. doi: 10.26749/rstpp.130.2.55

Shi, L., Xie, G. H., and Li, H. M. (1997). Trace element geochemistry of the volcanic rocks from the Taylor Valley and Ross Islands, Antarctica. *Geochimica* 13, 11. doi: 10.1088/0256-307X/16/9/027

Singer, A. (1984). The paleoclimatic interpretation of clay minerals in sediments—a review. *Earth Sci. Rev.* 21, 251–293. doi: 10.1016/0012-8252(84)90055-2

Stagg, H. M. J., Colwel, J. B., Direen, N. G., O'brien, P. E., Bernardel, G., Borissova, I., et al. (2004). Geology of the continental margin of Enderby and Mac. Robertson Lands, East Antarctica: insights from a regional data set. *Mar. Geophys. Res.* 25, 183–219. doi: 10.1007/s11001-005-1316-1

Stammerjohn, S. E., Maksym, T., Massom, R. A., Lowry, K. E., Arrigo, K. R., Yuan, X., et al. (2015). Seasonal sea ice changes in the Amundsen Sea, Antarctica, over the period of 1979–2014. *Elem.: Sci. Anthropocene* 3, 55. doi: 10.12952/journal.elementa.000055

Stiver, M., and Reimer, P. J. (1993). Extended ^{14}C data base and revised Calib 3.0 ^{14}C age calibration program. *Radiocarbon* 35, 215–230. doi: 10.1017/S0033822200013904

Suzuki, S., Hokada, T., Ishikawa, M., and Ishizuka, H. (1999). Geochemical study of granulites from Mt. Riiser-Larsen, Enderby Land, East Antarctica: Implication for protoliths of the Archean Napier Complex. *Polar Geosci.* 12, 101–125. doi: 10.15094/00003045

Takano, Y., Tyler, J. J., Kojima, H., Yokoyama, Y., Tanabe, Y., Sato, T., et al. (2012). Holocene lake development and glacial-isostatic uplift at Lake Skallen and Lake Oyako, Lützow-Holm Bay, East Antarctica: Based on biogeochemical facies and molecular signatures. *Appl. Geochem.* 27, 2546–2559. doi: 10.1016/j.apgeochem.2012.08.009

Taylor, S. R., and McLennan, S. M. (1985). The continental crust: its composition and evolution. *J. Geol.* 94, 57–72. doi: 10.1016/0031-9201(86)90093-2

Tingey, R. J. (1991). The regional geology of Archean and Proterozoic rocks in Antarctica. *geol. Antarctica*, 1–73. Available at: http://search.proquest.com/georef/docview/50177959/13223285216616C858/15?accountid=14245.

Trail, D. S., and McLeod, I. R. (1969). Geology of the Lambert Glacier region. In: C. Craddock (Editor), *Geologic Maps of Antarctica, 11* (Antarctic Map Folio Ser., 12). (Am. Geogr.Soc., New York).

Turner, J., Phillips, T., Marshall, G. J., Hosking, J. S., and Deb, P. (2017). Unprecedented springtime retreat of antarctic sea ice in 2016: Antarctic Sea ice retreat. *Geophys. Res. Lett* 44, 6868-6875. doi: 10.1002/2017GL073656

Wang, Z., Zhang, X., Guan, Z., Sun, B., Yang, X., and Liu, C. (2015). An atmospheric origin of the multi-decadal bipolar seesaw. *Sci. Rep.* 5 (8909), 1-5. doi: 10.1038/SREP08909

Williams, G. D., Nicol, S., Aoki, S., Meijers, A. J. S., Bindoff, N. L., Iijima, Y., et al. (2010). Surface oceanography of BROKE-West, along the Antarctic margin of the south-west Indian Ocean (30–80°E). *Deep Sea Res. Part II: Topical Stud. Oceanogr.* 57, 738–757. doi: 10.1016/j.dsr2.2009.04.020

Williams, G. D., Nicol, S., Raymond, B., and Meiners, K. (2008). Summertime mixed layer development in the marginal sea ice zone off the Mawson coast, East Antarctica. *Deep Sea Res. Part II: Topical Stud. Oceanogr.* 55, 365–376. doi: 10.1016/j.dsr2.2007.11.007

Wong, C. S., Whitney, F. A., Crawford, D. W., Iseki, K., Matear, R. J., Johnson, W. K., et al. (1999). Seasonal and interannual variability in particle fluxes of carbon, nitrogen and silicon from time series of sediment traps at Ocean Station P 1982–1993: relationship to changes in subarctic primary productivity. *Deep Sea Res. Part II: Topical Stud. Oceanogr.* 46, 2735–2760. doi: 10.1016/S0967-0645(99)00082-X

Xiu, C., Chen, X. X., Zhou, M. J., Meina, X., Zhang, X., and Xing, J. (2017). REE geochemical characteristics of core R11 in the Ross Sea Antarctic. *Mar. Geol. Front.* 33, 1–8. doi: 10.16028/j.1009-2722.2017.05001

Xu, F. J., Hu, B. Q., Zhao, J. T., Liu, X. T., Xu, K. H., Xiong, Z. F., et al. (2021). Provenance and weathering of sediments in the deep basin of the northern South China Sea during the last 38 kyr. *Mar. Geol.* 440, 106602. doi: 10.1016/j.margeo.2021.106602

Yang, J. Y., Jiang, F. Q., Yan, Y., Zheng, H., and Chang, F. M. (2022). Provenance and paleoclimatic significance of clay minerals from Izu-Ogasawara Ridge since Pliocene. *Earth Sci. Front.* 29, 73–83. doi: 10.13745/j.esf.sf.2022.1.8

Yemane, K., Kahr, G., and Kelts, K. (1996). Imprints of post-glacial climates and palaeogeography in the detrital clay mineral assemblages of an Upper Permian fluviolacustrine Gondwana deposit from northern Malaw. *Palaeogeogr. Palaeoclimatol. Palaeoecol.* 125, 27–49. doi: 10.1016/S0031-0182(96)00023-5

Yoshida, Y., and Moriwaki, K. (1979). *Some consideration on elevated coastal features and their dates around syowa station, Antarctica* (Memoirs of National Institute of Polar Research) 13, 220–226.

Zhang, J. R. (2011). Element features in different grain size fractions of lacustrine sediment and their environmental implication: A case study of Huangqihai Lake. *Acta Sedimentol. Sin.* 29, 381–387. doi: 10.1007/s11589-011-0776-4